Journal of ELECTRICAL ENGINEERING, VOL 73(2022), NO6, 368–377

sciendo

PAPERS

De-noising of partial discharge ultrasonic signal of insulation bar in large motor based on GMC-wavelet

Xuejun Chen[1,*], Lin Ma[2], Lei Zhang[3], Jianhuang Zhuang[4]

In view of the bad operation environment of large motor, which often suffers from various strong noise interference, the partial discharge ultrasonic signal is often annihilated, which makes it difficult to detect and analyse. A de-noising method based on generalized minimax concavity (GMC) and wavelet for partial discharge (PD) ultrasonic signal is proposed. GMC is used to enhance the sparsity of PD ultrasonic signal and eliminate the high-frequency noise signal at the same time. Then the residual high-frequency sparse noise and low-frequency noise of the former are de-noised again combined with wavelet. Finally, the signal is reconstructed to achieve the purpose of de-noising the original PD ultrasonic signal with noise. Compared with ℓ_1-norm method, GMC method, wavelet method and ℓ_1-norm-wavelet method, the simulation results show that based on time domain analysis, the de-noising effect of the proposed method is obviously better than the other four methods. The SNR and MSE of the former are better than those of the latter. In addition, the insulation bar discharge model of large motor is constructed to obtain the actual PD ultrasonic signal, which further verifies its effectiveness, and its de-noising effect is also better than the four methods. This method can not only enhance the sparsity of the target signal and improve the estimation accuracy, but also achieve the de-noising effect, while retaining the effective information of PD ultrasonic signal characteristics. This method can provide new ideas for other types of PD signal de-noising, and lay the foundation for later feature analysis.

K e y w o r d s: insulation, generalized minimax concave, partial discharge, ultrasonic, de-noising

1 Introduction

With the rapid development of power system, the number of large electrical equipment is increasing, which makes the maintenance of power equipment more and more difficult. How to ensure the maintenance without affecting the operation of power system or single machine off grid, detection methods and fault diagnosis have become the key technical problems.

Partial discharge (PD) detection is one of the important means to supervise the insulation performance of electrical equipment. Many scholars have proposed current, ultrasonic, ultra-high frequency, optical detection methods for PD detection and fault diagnosis [1]. Among them, because of its propagation characteristics and audio frequency characteristics, ultrasound is favored and mature for PD detection and discharge source positioning in transformers, switch cabinets, *etc*, [2-3].

However, for large motor PD, current deteection method is usually used. However, when the PD of large motor is known to exceed the standard, the current method is often unable to determine the specific part of the PD source, so it is necessary to disassemble it, and even find and confirm the source of PD for each insulated bar. It will waste a lot of manpower, material and financial resources to dismantle on site. With the help of ultrasonic characteristics and positioning of PD, the position of PD can be reduced initially, and even the purpose of positioning can be achieved. However, the operation environment of large motor is usually bad, and it is easy to suffer from various strong noise interference, and the attenuation is large in the dielectric propagation, which is often buried by strong noise, resulting in the difficulty of PD ultrasonic detection [4]. Therefore, it is urgent to de-noise the detected PD Ultrasonic.

In signal noise processing, many methods have been studied and applied. The traditional filtering method has good filtering effect for stationary signal, but it fails in non-stationary and non-linear signal, and even leads to signal distortion. For this reason, many scholars have proposed filtering methods such as wavelet, independent component analysis, adaptive, singular value decomposition, empirical mode decomposition, particles, and sparseness [5-11].

On the basis of singular value decomposition, adaptive singular value decomposition (SVD) is proposed in reference [12] to suppress the noise of PD. However, with the decrease of signal-to-noise ratio, it becomes difficult to determine the threshold and the de-noising effect becomes poor. In order to overcome these problems, one

[1] Key Laboratory of Fujian Universities for New Energy Equipment Testing, Putian University, Putian, 351100, P.R. China, [2] School of Mechanical Engineering and Automation, Fuzhou University, Fuzhou 350108, PR China, [3] College of Mechanical and Electrical Engineering, Fujian Agriculture and Forestry University, Fuzhou 350100, PR China, [4] Putian power supply company of State Grid Fujian Electric Power Co., Ltd, Putian 351100, PR China, Correspondence information*: Key Laboratory of Fujian Universities for New Energy Equipment Testing, Putian University, Putian, 351100, P.R. China, cxjnet@126.com

https://doi.org/10.2478/jee-2022-0051, Print (till 2015) ISSN 1335-3632, On-line ISSN 1339-309X

method intercepts the noisy PD signal through the short-term data window, and uses singular value decomposition to eliminate the noise data, which is better than wavelet analysis and singular value decomposition, but the de-noising effect of this short-term singular value decomposition is affected by the length of sliding data window [13].

Due to its adaptive decomposition characteristics, empirical mode decomposition (EMD) has been applied to nonlinear signal de-noising and achieved good de-noising effect, but there are still many problems to be solved, such as how to solve the modal aliasing and select the de-noising modal components [14]. All kinds of wavelet de-noising methods are also used in PD signal processing, and vibration signals of rotating machines, and in many cases, the effect is obviously better than other filtering methods, [15-17]. However, the effect of wavelet de-noising is often limited by wavelet function selection and parameter determination [18-20].

Because the high-frequency part of the signal in nature is mostly noise, Donoho et al. proposed to use sparsity to eliminate the high-frequency part of the noise [21]. Selesnick proposed a nonconvex regularization term, whose sparsity is better than standard convexity. Group sparse signal de-noising has achieved good results in signal-to-noise ratio (SNR) and perceptual quality [22]. Sparse method has become a research hotspot because of its advantages of reducing data dimension and wide range of signal representation. It is widely used in image and signal de-noising, compression, recognition and other fields. At the same time, it is also used in PD signal de-noising [23-25].

In order to enhance the sparsity and estimation accuracy of the target, generalized minimax concavity (GMC) is proposed to induce nonconvex penalty function by sparsity, which avoids the underestimation of -norm regularization [26]. This method is quickly applied to the de-noising of mechanical fault diagnosis signal, and the effect is better than that based on -norm and other methods [27]. Goswami manifested the minimization of the ℓ_1-error objective function by using a hybrid optimization technique consisting of the particle swarm and simulated annealing optimization algorithm. But it is only used for design of a differentiator in the digital domain [28]. However, in the application of GMC to ECG de-noising, the SNR and root mean square error (RMSE) based on -norm have been significantly improved [29].

The PD ultrasonic signal of a large motor with noise is a typical non-stationary mixed signal. In this paper, a de-noising method based on GMC-wavelet is proposed. GMC is used to de-noise the PD ultrasonic signal sparsely, and then wavelet is used to de-noise the remaining part of the sparse noise. Finally, signal reconstruction is carried out to achieve the purpose of de-noising the original noisy PD ultrasonic signal.

2 De-noising method

2.1 Sparse model and optimal solution

Assume that the $y \in \mathcal{R}^M$ model of the observed noisy signal is

$$y = Ax + n. \tag{1}$$

Among them, $x \in \mathcal{R}^N$ is the original signal to be extracted, $A \in \mathcal{R}^{M\times N}$ is a known linear operator, and $n \in \mathcal{R}^M$ is Gaussian white noise. To obtain the original signal x, the sparse reconstruction algorithm can be used to solve (1), so as to achieve the purpose of de-noising.

The convex optimization method based on ℓ_1-norm is commonly used in sparse reconstruction. The method is to minimize the regularized linear least squares loss function [26], namely

$$\min \frac{1}{2}\|y - Ax\|_2^2 + \lambda\varphi(x). \tag{2}$$

In (2), λ is a regularization parameter, and φ is a regularizer. In this case, the ℓ_1-norm is usually used as a regularizer because it reduces the sparsity most effectively in the convex regularizer.

When the penalty term is ℓ_1-norm, the iterative soft threshold algorithm can be used to solve (2). The iterative equation is

$$x^{i+1} = f_{\lambda\mu}(x^i - uA^H y - Ax^i), \tag{3}$$

where $f_{\lambda\mu}$ is the soft threshold function

$$f_{\lambda\mu}(x) = \begin{cases} \operatorname{sign}(x)(x - \lambda\mu), & \text{if } |x| \geq \lambda\mu \\ 0, & \text{if } |x| < \lambda\mu \end{cases}. \tag{4}$$

Among them, μ is the control convergence parameter, that is $0 < \mu < \|A\|_2^{-2}$, sign is the signum function.

GMC can be regarded as a multivariate generalization of the minimax-concave (MC) penalty function. It uses the Huber function s, see below, for multivariate realization, which can not only avoid the underestimation characteristics caused by the ℓ_1-norm regularization solution, but also enhance the sparsity of the target [26-27,29]

$$s_b(x) = s(b^2x)/b^2, \quad b \neq 0, \tag{5}$$

where $b \in \mathcal{R}$ is a scale variable and an univariate Huber function is

$$s_b(x) = \begin{cases} \frac{1}{2}x^2, & \text{if } |x| \leq 1 \\ |x| - \frac{1}{2}, & \text{if } |x| \geq 1 \end{cases}. \tag{6}$$

If $b = 0$, then $S_o = 0$, hence if $b \neq 0$, the variable scale Huber function is

$$s_b(x) = \begin{cases} \frac{1}{2}b^2x^2, & \text{if } |x| \leq 1/b^2 \\ |x| - \frac{1}{2b^2}, & \text{if } |x| \geq 1/b^2 \end{cases}. \tag{7}$$

According to Huber function, the variable scale minimax concave penalty function is

$$\varphi_b(x) = |x| - s_b(x). \tag{8}$$

If the matrix $B \in \mathcal{R}^{M\times N}$, the multivariate generalized $\varphi_B(x)$ of the variable-scale minimum-maximum concave penalty function can be obtained, that is, the generalized minimum-maximum concave penalty function GMC

$$\varphi_B(x) = \|x\|_1 - s_B(x). \tag{9}$$

Among them, $s_B(x)$ is a multivariate extension of Huber function, and

$$s_B(x) = \inf_{v\in\mathcal{R}^N} \|v\|_1 + \frac{1}{2}\|B(x-v)\|_2^2\}. \tag{10}$$

Among them, v is a point in the field of x. For a given $B \in \mathcal{R}^{M\times N}$, the GMC penalty function satisfies

$$\varphi_B(x) = \|x\|_1 - \frac{1}{2}\|Bx\|_2^2, \qquad \|B^H Bx\|_\infty \le 1. \tag{11}$$

This shows that the GMC penalty function approximates the ℓ_1-norm around 0. which is

$$\varphi_B(x) = \|x\|_1, \qquad x \approx 0. \tag{12}$$

How to set GMC penalty function to keep regularized convex least squares loss function is considered. The objective function of sparse regularization is constructed

$$F(x) = \frac{1}{2}\|y - Ax\|_2^2 + \lambda\varphi_B(x), \tag{13}$$

where φ_B satisfies the penalty function of (9), if

$$B^H B \le \frac{1}{\lambda}A^H A, \tag{14}$$

so F is a strictly convex function. In order to satisfy the convex condition of (14), let

$$B = \sqrt{\gamma/\lambda}A, \qquad 0 \le \gamma \le 1. \tag{15}$$

When $\gamma \le 1$, $B^H B \le (\gamma/\lambda t)A^H A$ satisfies (14). Parameter γ controls the non-convexity of the penalty function φ_B. When $\gamma = 0$, then $B = 0$, and the penalty function is reduced to the L_1 norm; when $\gamma = 1$, the penalty function is non-convex to the maximum. In practice, $0.5 \le \gamma \le 0.8$ is usually taken.

The purpose of de-noising is achieved by solving the convex optimization problem of (13). When B satisfies (14), the near end algorithm can be used to minimize the objective function F, that is, the optimal convex solution of F is transformed into a saddle point problem [26-27,29]:

$$(x^{\text{opt}}, y^{\text{opt}}) = \arg \min_{x\in\mathcal{R}^N} \max_{v\in\mathcal{R}^N} \left\{\frac{1}{2}\|y - Ax\|_2^2 + \lambda\|x\|_1 - \lambda\|v|_1 - \frac{\lambda}{2}\|B(x-v)\|_2^2\right\}. \tag{16}$$

The saddle point problem is an example of monotone inclusion problem. Therefore, forward backward (FB) algorithm can be used to solve this problem. FB algorithm only involves simple calculation steps as follows

1) Input y, A, λ, γ;

2) Initialize $\rho = \max\{1, \gamma/(1-\gamma)\|A^H A\|_2\}, 0 < \mu < 2/\rho$;

3) For $i = 0, 1, 2, \cdots$, the iteration is as follows

$\omega^i = x^i - \mu A^H \left(A(x^i + \gamma(v^i - x^i)) - y\right)$,

$u^i = v^i - \mu\gamma A^H A \left(v^i - x^i\right)$,

$x^{i+1} = f_{\lambda\mu}\left(\omega^i\right)$,

$v^{i+1} = f_{\lambda\mu}\left(u^i\right)$;

iterate until convergence, then output x, and get the original signal to be extracted.

2.2 Wavelet de-noising

For the observed noisy signal $y = x + n$, the original signal is x and the noise is Gaussian white noise n.

The unbiased risk estimation threshold in wavelet de-noising theory is adopted, that is, each coefficient of signal y wavelet decomposition is taken as absolute value, then sorted in ascending order and squared to obtain a new sequence $W = [\{w_1\}, \{w_2\}, \cdots, \{w_N\}]$, and the unbiased risk estimation threshold can be defined as

$$r_k = \sqrt{w_{k\min}}. \tag{17}$$

Among them, $w_{k\min}$ is the minimum risk point of the risk curve $R_{\text{ish}}(k))$

$$R_{\text{ish}}(k) =]\frac{1}{N}\left[N - 2k + \left(N-k\right)w_k + \sum_{i=1}^{k} w_i\right] \tag{18}$$

$k = 1, 2, \cdots, N$. Here, because the signal after GMC de-noising still contains some sparse noise, the wavelet threshold here is adjusted according to the noise level estimation of each layer of wavelet decomposition.

2.3 De-noising method based on GMC-wavelet

Electrical equipment usually has serious environmental noise interference, and the PD ultrasonic signal is weak. After GMC de-noising, the signal also contains some sparse noise. In order to improve the de-noising ability, wavelet de-noising is introduced, and a PD ultrasonic signal de-noising method based on GMC-wavelet is proposed.

In this de-noising method, GMC is used to enhance the PD ultrasonic signal sparsely to eliminate the noise. Then unbiased estimation is used based on wavelet, and the noise level estimation is adjusted according to the wavelet decomposition to achieve the sparse noise de-noising. Finally, the results of wavelet de-noising are reconstructed to obtain the de-noised PD ultrasonic signal. The de-noising process is shown in Fig. 1.

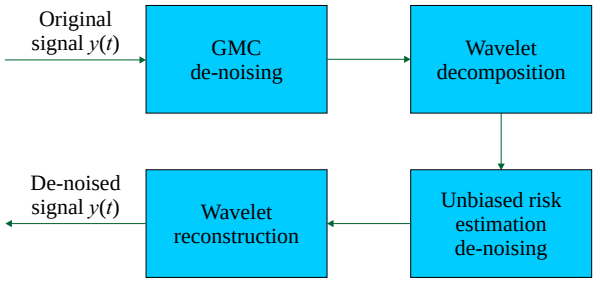

Fig. 1. The Principle block diagram of de-noising method based on GMC-wavelet

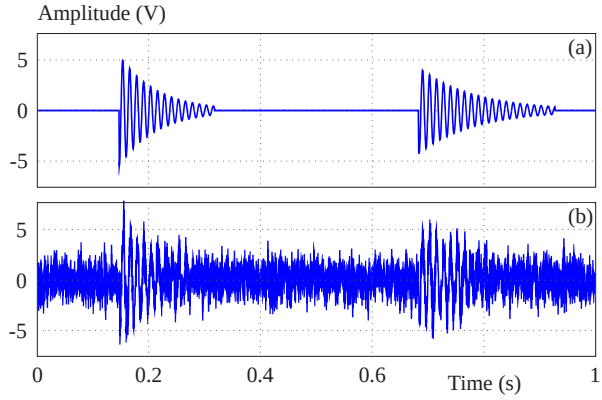

Fig. 2. Simulation, signal $x(t)$: (a) – without noise, (b) – with noise

3 De-noising and analysis of simulation signal

Due to the long-term operation of large motor in strong electromagnetic interference environment and other noise interference, the PD ultrasonic signal generated by insulation is often weak and submerged in the noise, which is not conducive to the analysis and processing of PD ultrasonic signal. It is difficult to verify the de-noising effectiveness of the proposed method based on GMC-wavelet if the actual PD ultrasonic signal is directly used. Therefore, a simulated mixed signal $x(t)$ is designed, which is composed of two exponential oscillation attenuation signals

$$x(t) = \begin{cases} 50\, e^{-15t} \sin(160\pi t), & \text{if } 0.146 \leq t \leq 0.317, \\ 4000\, e^{-10t} \sin(160\pi t), & \text{if } 0.684 \leq t \leq 0.928, \\ 0, \quad \text{otherwise.} \end{cases} \tag{19}$$

The mixed simulation signal is shown in Fig. 2(a). Then the $x(t)$ is superimposed with the Gaussian white noise signal with the mean value of 0 and the standard deviation of 1, and the $x(t)$ mixed simulation signal with noise is shown in Fig. 2(b).

To intuitively analyze the de-noising effect based on GMC-wavelet, and compare with GMC de-noising, ℓ_1-norm de-noising, wavelet de-noising, and ℓ_1-norm-wavelet de-noising, these methods are applied to de-noise in Fig. 2(b), and the waveform after de-noising is shown in Fig. 3. As can be seen from Fig. 3(a)-(c), compared with Fig. 2(b), the waveform based on ℓ_1-norm, GMC-wavelet de-noising has achieved a great degree of de-noising effect. However, in terms of waveform, Fig. 3 (a) contains more high-frequency noise than (b) and (c), and Fig. 3(c) has the least high-frequency noise after wavelet de-noising. Figure 3(d) is the waveform after de-noising based on ℓ_1-norm-wavelet, which shows less high-frequency noise than Fig. 3(a), indicating that the de-noising effect based on ℓ_1-norm-wavelet is better than that based on ℓ_1-norm. Similarly, it can be seen that the de-noising effect based on GMC-wavelet in Fig. 3(e) is obviously better than that based on GMC.

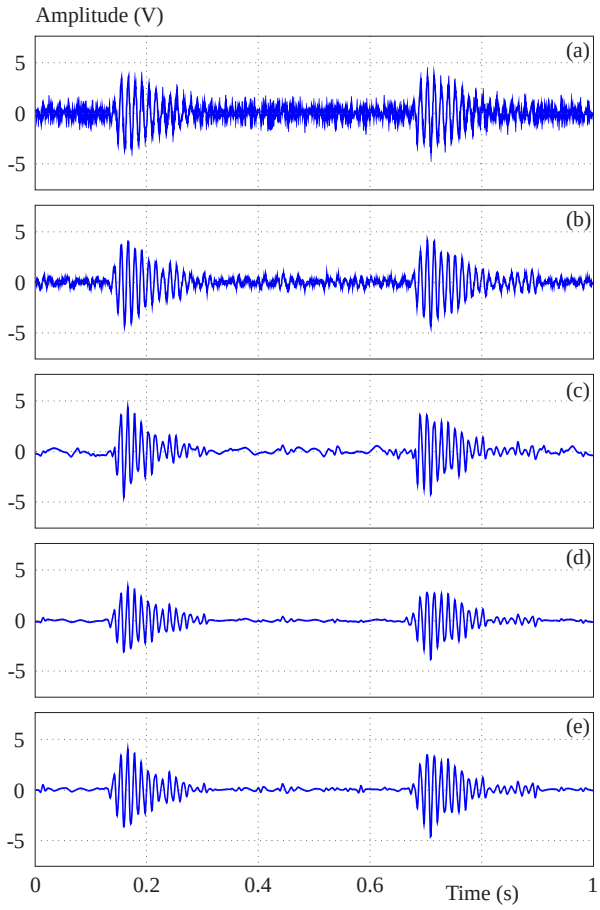

Fig. 3. The waveform of simulation signal $x(t)$ with noise after de-noising based on: (a) – ℓ_1-norm, (b) – GMC, (c) – wavelet, (d) – ℓ_1-norm wavelet, and (e) – GMC-wavelet

To further observe the frequency domain changes of the signal before and after de-noising, fast Fourier transform is performed on Fig. 2(b) and Fig. 3(a)-(e) respectively to obtain the spectrum of the corresponding signal, as shown in Fig. 4. It can be seen in (a) that the main frequency spectrum value of the original simulation signal $x(t)$ with noise is 80Hz, which is the same as that of the simulation signal $x(t)$, but it is accompanied by a strong noise spectrum value in the whole frequency domain. Fig. 4(b) is the Fourier spectrum of the waveform after ℓ_1-norm de-noising. Compared with Fig. 4(a), the

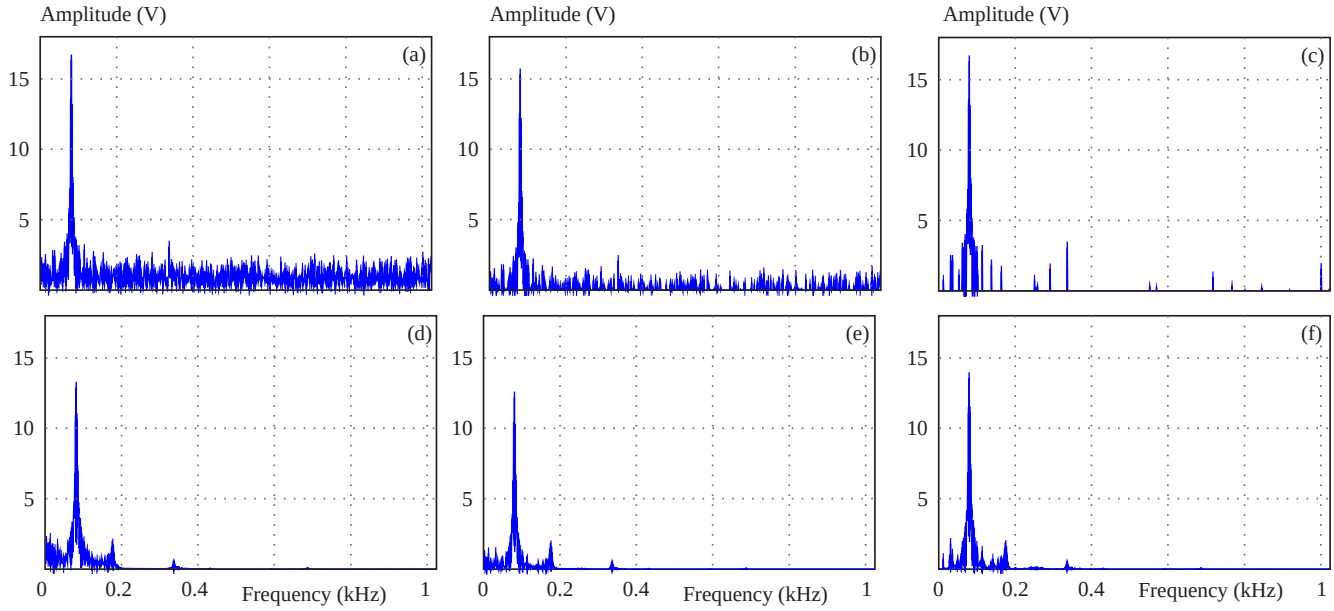

Fig. 4. The Fourier spectrum of: (a) – original signal with noise, (b) – de-noised using ℓ_1-norm, (c) – GMC, (d) – wavelet, (e) – ℓ_1-norm wavelet, and (f) – GMC-wavelet

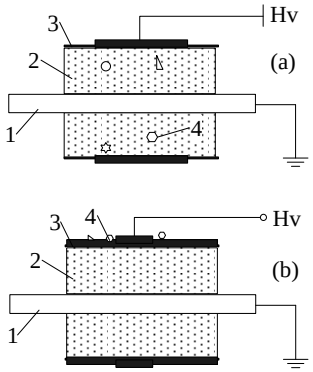

Fig. 5. Experiment model of PD: (a) – (1-bar conductor, 2-main insulation, 3-anti-corona layer, 4-internal air gap), (b) – (1-bar conductor, 2-main insulation, 3-anti-corona layer, 4-oil contamination)

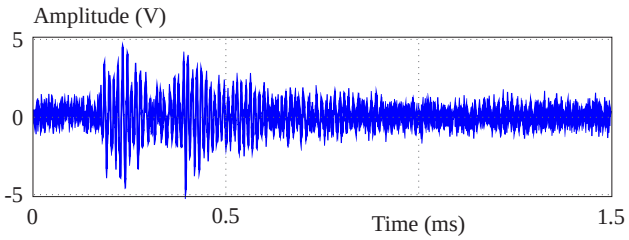

Fig. 6. The ultrasonic original signal of PD in insulation

main value of the spectrum is kept at 80Hz, and the noise in other frequency domains is weakened, which is consistent with the time domain de-noising effect in Fig. 3(a). Figure 4(c) is the Fourier spectrum of the waveform after GMC de-noising. It also keeps the main value of the spectrum at 80Hz. Compared with Fig. 4(a) and (b), the noise in other frequency bands is almost eliminated, and there are only some sparse single spectrum values. Comparatively speaking, the de-noising effect is better than that based on ℓ_1-norm. Fig. 4(d) is the Fourier spectrum of the waveform after de-noising based on wavelet. Its high-frequency noise almost does not exist, but compared with Fig. 4(b) and (c), the low-frequency noise elimination is weak.

Figure 4(e) is the Fourier spectrum of the waveform after de-noising based on ℓ_1-norm-wavelet. Compared with Fig. 4(b), the high-frequency noise is almost eliminated, and the low-frequency noise is also weakened a lot; the principal value of 80Hz spectrum is also a little smaller, because the noise is superimposed on the principal spectrum, which is also eliminated at this time. Figure 4(f) is the Fourier spectrum of the waveform after GMC-wavelet de-noising. Compared with Fig. 4(c), the sparse single spectrum value in the high frequency band is almost eliminated; compared with Fig. 4(e), the noise in the low frequency band is also weakened.

Table 1. Comparisons of de-noising results of the five methods

Method	SNR(dB)	RMSE
ℓ_1-norm	7.48	0.42
GMC	8.31	0.38
wavelet	8.11	0.39
-norm-wavelet	8.04	0.39
GMC-wavelet	8.74	0.36

From the comparison and analysis of the above time-frequency waveforms, it can be seen that the de-noising effect based on GMC-wavelet is better than other several de-noising methods.

To quantitatively evaluate the de-noising effect of the five methods, SNR and RMSE are introduced as evaluation indexes to measure the de-noising effect of the

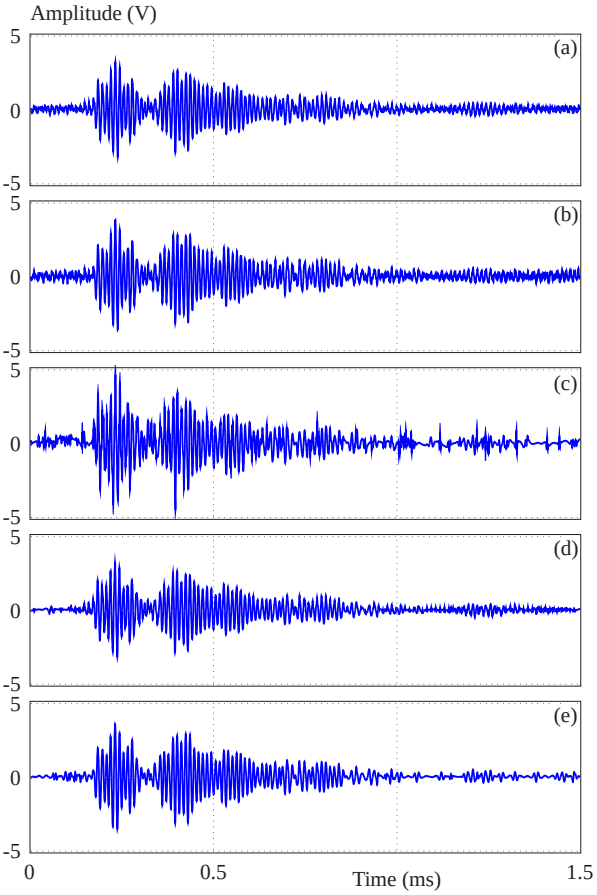

Fig. 7. The waveform of ultrasonic original signal of PD in insulation after de-noising based on: (a) – ℓ_1-norm, (b) – GMC, (c) – wavelet, (d) – ℓ_1-norm wavelet, and (e) – GMC-wavelet

original noisy simulation signal $x(t)$. Through the experimental calculation, the evaluation index results after five methods of de-noising are shown in Tab. 1.

It can be seen that the SNR value after GMC-wavelet base de-noising is the largest and the RMSE value is the smallest, indicating the best de-noising effect. The SNR value based on ℓ_1-norm is the smallest, the RMSE value is the largest, and the de-noising effect is the worst, which is consistent with the time domain analysis of Fig. 3 and Fig. 4. The SNR values based on GMC and wavelet respectively are larger than those based on ℓ_1-norm-wavelet, and the SNR value based on GMC is larger than that based on wavelet, while the corresponding RMSE value is on the contrary, which shows that the de-noising effect based on ℓ_1-norm-wavelet is not better than that based on simple wavelet. In addition, after many experiments, the five de-noising methods for different simulation signal de-noising analysis results will change, but the effect is still based on GMC-wavelet de-noising method is the best.

4 De-noising analysis of PD ultrasonic signal

In order to verify the de-noising effect of the proposed de-noising method, two kinds of PD models of large motor are adopted for experimental verification, namely internal discharge and end discharge of winding insulator, as shown in Fig. 5 [7-11]. Figure 5(a) is the internal discharge model of winding insulator, which simulates the air gap in the insulation bar due to manufacturing process problems. These air gaps are operated under high pressure and other environments for a long time, and it is easy to reach the breakdown field strength and lead to PD, which further reduces the insulation strength and makes the insulation damage or breakdown. Fig. 5(b) is the end discharge model. There are oil pollutants on the surface of the end discharge model, which reduces the surface insulation strength and is easy to produce surface PD. The

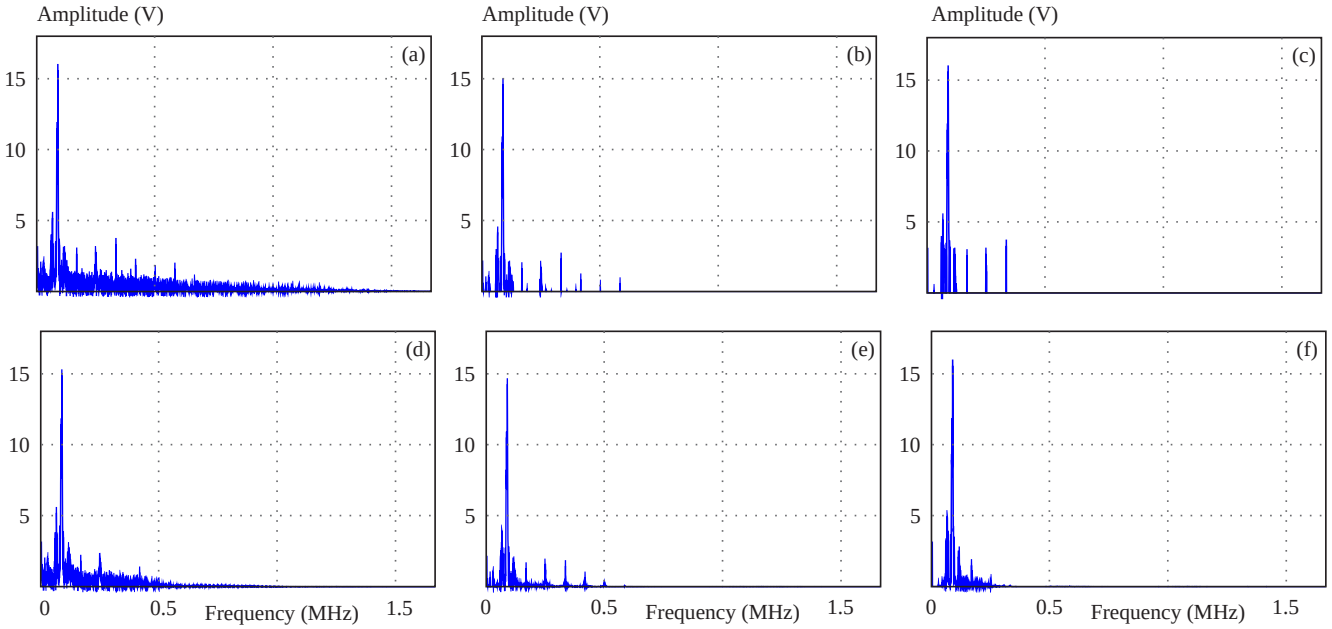

Fig. 8. The Fourier spectrum of ultrasonic signal of PD in insulation (a) – original signal, after de-noising: (b) – ℓ_1-norm, (c) – GMC, (d) – wavelet, (e) – ℓ_1-norm wavelet, and (f) – GMC-wavelet

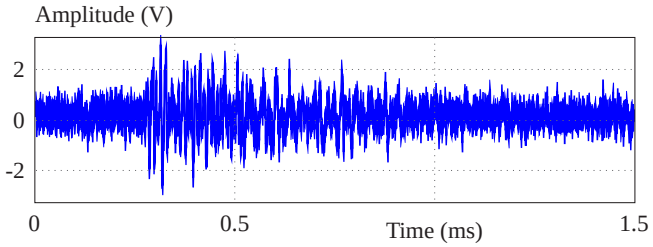

Fig. 9. The ultrasonic original signal of PD on end surface

two PD models are made of single bar of 36 MW/4 KV generator.

The ultrasonic sensor used is made of PZT sensitive elements, with a frequency response range of 20–200kHz. Then through 100 times the signal gain, the PD ultrasonic signal is acquired by the oscilloscope.

According to the internal discharge model in Fig. 5(a), by adjusting the Hv end of the step-up transformer, when the voltage rises to 2.5KV, the oscilloscope adopts the PD ultrasonic signal, as shown in Fig. 6. It can be seen from Fig. 6 that the PD ultrasonic signal contains strong noise and two strong PD impulse signals.

Similar to the above analysis of the simulation signal containing noise, the noise of the PD ultrasonic signal in the insulation in Fig. 6 is also eliminated based on ℓ_1-norm de-noising, GMC de-noising, wavelet de-noising, ℓ_1-norm-wavelet de-noising and GMC-wavelet de-noising, and the de-noised results are shown in Fig. 7(a)-(e). Because the signal in Fig. 6 is the actual PD ultrasonic signal, due to the experimental environment and detection equipment and other factors, it is impossible to obtain the ideal original PD ultrasonic signal without noise. Therefore, SNR and RMSE cannot be used to compare the de-noising effects of the five methods qualitatively and quantitatively.

However, the de-noising time-frequency diagram can still be used to qualitatively evaluate the de-noising effect. Compared with Fig. 6, the noise amplitude in Fig. 7(a) is obviously smaller in the time domain without PD ultrasonic signal, and the amplitude of PD signal is also relatively smaller, because it is also superimposed with noise and eliminated. In Fig. 7(b) and(c), compared with Fig. 6, similarly, in the time domain without PD, the noise amplitude is obviously smaller, and in some time domain, the noise in Fig. 7(c) is completely eliminated. The noise amplitude of Fig. 7(d) is smaller than that of Fig. 7(a). Similarly, the noise amplitude of Fig. 7(e) is smaller than that of Fig. 7(b), and some noises no longer exist. It shows that the de-noising effect based on -norm-wavelet and GMC-wavelet is better than that based on ℓ_1-norm and GMC respectively.

To further analyze the de-noising effect from the frequency domain, Fourier transform is performed on each waveform in Fig. 7 to obtain the signal spectrum, as shown in Fig. 8, respectively. It can be seen from Fig. 8 that the dominant frequency of PD ultrasound in the insulation is about 85 kHz. In Fig. 8(b) and(c), compared with Fig. 8(a), there are only a few sparse spectral values in the high frequency band, and there are almost no spectral values in the low frequency band of Fig. 8(c). Compared with Fig. 8(a), the high-frequency frequency spectrum in Fig. 8(d) does not exist, but there are more spectrum values near the main frequency spectrum value compared with Fig. 8(b) and(c), which shows that the de-noising effect based on wavelet is not as good as the other two methods near the main frequency value. Compared with Fig. 8(b), the sparse spectrum value of other frequency bands in Fig. 8(e) is smaller, which shows that the de-noising effect based on ℓ_1-norm-wavelet is better than that based on -norm. Compared with Fig. 8(c) and other spectrums, Fig. 8(f) has almost only the main frequency spectrum value, which indicates that the original noise is almost completely eliminated after GMC-wavelet de-noising.

To verify the de-noising effect of different actual PD ultrasonic signals, the experimental object made of the end surface discharge model in Fig. 5(b) is used. Similarly, by adjusting the Hv end of the step-up transformer, when the voltage rises to 3.3 kV, the oscilloscope adopts the PD ultrasonic signal, as shown in Fig. 9. It can be seen from Fig. 9 that the PD ultrasonic signal also contains strong noise and a strong PD impulse signal.

Similarly, the PD ultrasonic signal of end surface in Fig. 9 is de-noised based on ℓ_1-norm, GMC, wavelet, ℓ_1-norm-wavelet and GMC-wavelet. The de-noised waveforms are shown in Fig. 10(a) -(e) respectively. At the same time, the Fourier transform is performed on each waveform in Fig. 10 to obtain each spectrum, as shown in Fig. 11.

It can be seen from Fig. 10 that compared with Fig. 9, the waveforms de-noised by the five methods are obviously smaller in the time domain except for the PD signal, which indicates that the five methods are also effective in de-noising the ultrasonic signal of PD on the end surface. It can be seen from Fig. 11 that there are several main frequency values of the signal, and there are larger spectrum values in the frequency domain of 30 kHz, 60 kHz and 90 kHz respectively. Compared with Fig. 8, it shows that the spectrum characteristics of different types of PD ultrasonic signals are different.

Compared with Fig. 8(d), the noise amplitude in Fig. 8(b) and(c) is almost nonexistent near the main frequency spectrum, which indicates that the de-noising effect based on ℓ_1-norm and GMC is better than that of wavelet. Compared with Fig. 8(b) and(c), Fig. 8(e) and(f) have no sparse spectrum value in high frequency band, that is, high frequency noise is eliminated, which is the same as the de-noising effect of internal PD ultrasonic signal, indicating that the de-noising effect based on GMC-wavelet and ℓ_1-norm-wavelet is better than that based on ℓ_1-norm and GMC. The main frequency spectrum value in Fig. 8(e) is larger than that in(f), which indicates that GMC-wavelet is better than ℓ_1-norm-wavelet to keep the original signal.

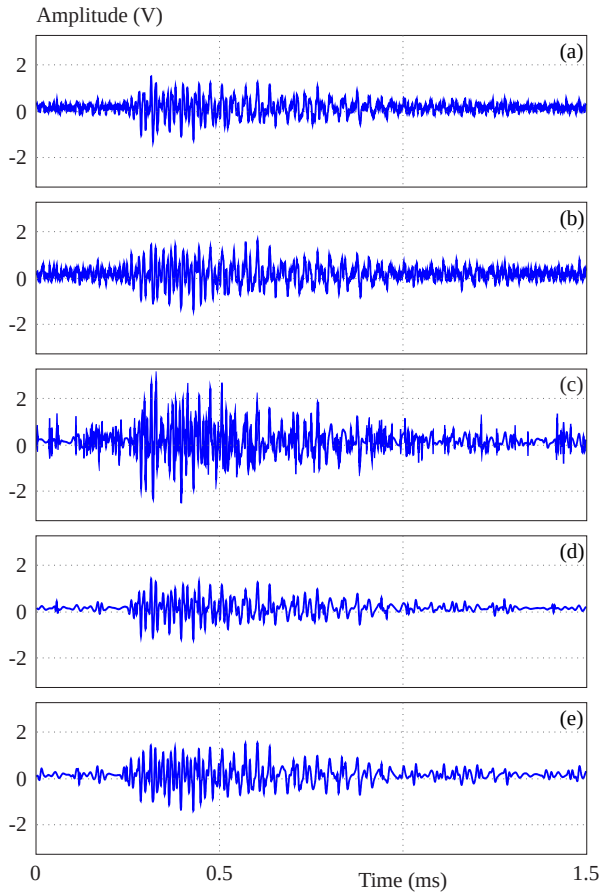

Fig. 10. The waveform of ultrasonic original signal of PD on end surface after de-noising based on: (a) – ℓ_1-norm, (b) – GMC, (c) – wavelet, (d) – ℓ_1-norm wavelet, and (e) – GMC-wavelet

Combined with the analysis of the de-noising effect of the noise simulation signal, the actual PD ultrasonic signal de-noising effect of the five methods has changed, but the GMC-wavelet de-noising effect is the best. It not only eliminates most of the noise components, but also best retains the effective information of the original signal. It can be seen that the effect of GMC-wavelet de-noising method on different signals is different, but the performance of noise elimination remains unchanged.

During the experiment, it is found that the unbiased likelihood estimation threshold rule of the wavelet is conservative. When a small part of the high-frequency information of the noisy signal is in the noise range, this threshold is very useful and can extract weak signals. Unbiased likelihood estimation is an adaptive wide value selection. Although the overall continuity is good, unbiased likelihood estimation requires a given threshold, and there is always a constant deviation between the estimated value and the actual value, and the derivative of the soft threshold function is discontinuous, which has certain limitations. The wavelet function is not unique, and can only be selected and determined through continuous experiments. In addition, the regularization parameter and the maximum eigenvalue of the generalized minimax concave(GMC) also need to be selected.

5 Conclusions

PD ultrasonic signals often contain strong noise due to the influence of the detection environment, which is unfavorable for ultrasonic signal feature analysis and insulation performance diagnosis. Aiming at the non-linear and non-stationary characteristics of PD signals, a denoising method for PD ultrasonic signals of large motors based on GMC-wavelet is proposed. Compared with the ℓ_1-norm, GMC avoids the system underestimation characteristic of ℓ_1-norm regularization, and further increases the sparsity of the objective function. In addi-

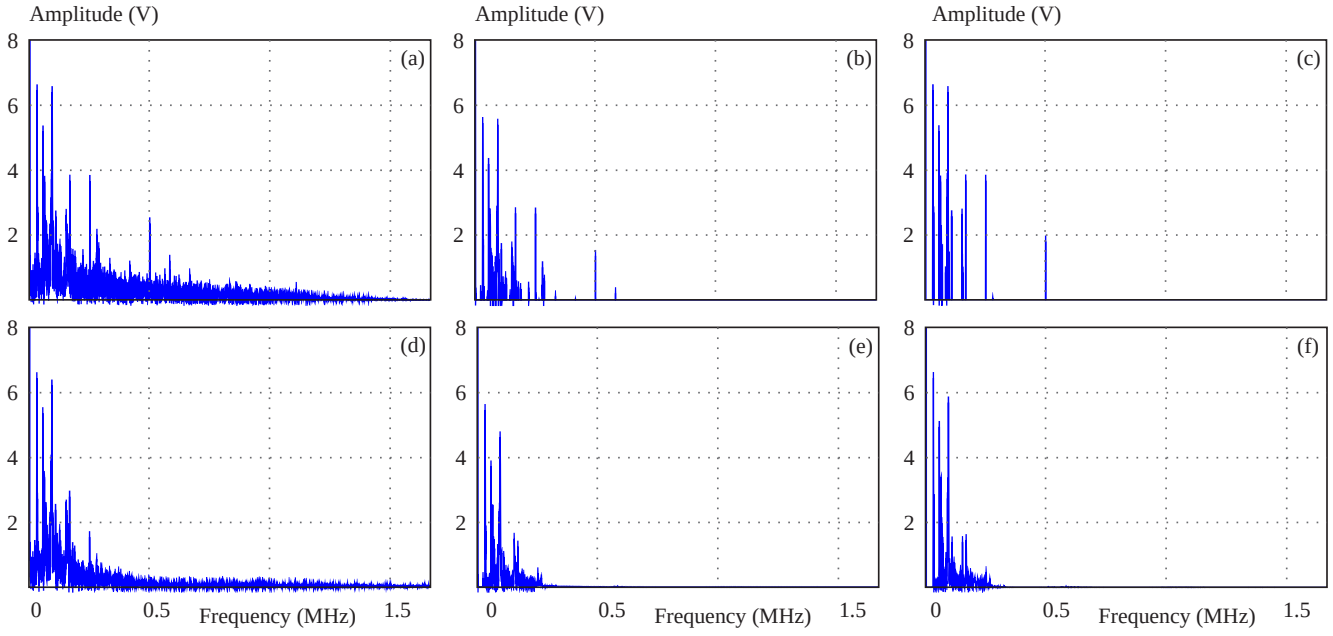

Fig. 11. The Fourier spectrum of ultrasonic signal of PD on end surface (a) – original signal, after de-noising: (b) – ℓ_1-norm, (c) – GMC, (d) – wavelet, (e) – ℓ_1-norm wavelet, and (f) – GMC-wavelet

tion, combined with wavelet, the remaining sparse high-frequency noise and low-frequency noise are effectively removed. Compared with the de-noising effect of ℓ_1-norm method, GMC method, wavelet method and ℓ_1-norm-wavelet method for PD ultrasonic simulation signals and test model signals, the SNR and RMSE of the proposed method after de-noising are the best. It not only eliminates high-frequency noise, but also eliminates low-frequency noise, but also retains the effective information of PD ultrasonic signals, which can provide a new idea for noise elimination of other types of PD ultrasonic signals.

Acknowledgements This work is supported by the Natural Science Foundation of Fujian Province of China (2022J011169), and the Program for New Century Excellent Talents in Fujian Province University (2018047). All data included in this study are available upon request by contact with the corresponding author.

References

[1] J. Li, X. Han, Z. Liu, and Y. Li, "Review on partial discharge measurement technology of electrical equipment", *High Voltage Engineering*, vol. 41, no. 8, pp. 2583-2601, 2015.

[2] L. Tang, R. Luo, M. Deng, and J. Su, "Study of Partial Discharge Localization Using Ultrasonics in Power Transformer Based on Particle Swarm Optimization", *IEEE Transactions on Dielectrics and Electrical Insulation*, vol. 15, no. 2, pp. 492-495, 2008.

[3] D. Li, J. Yang, J. Liang, and L. Wu, "Characteristics of acoustic signal form free moving metallic particles in gas insulated swithchgear", *Journal of Xi'an Jiaotong University*, vol. 43, no. 2, pp. 101-105, 2009.

[4] D. Zheng and P. Zhang, "A review of fault diagnosis and online condition monitoring of stator insulation in AC electrical machine", *Proceedings of the CSEE*.

[5] X. Luo, H. Niu and L. Lai, "Application of adaptive wavelet neural network based on particle swarm optimization algorithm in online PD pattern recognition", *Transactions of China Electrotechnical Society*, vol. 29, no. 10, pp. 326-333, 2014.

[6] Y. Qian, C. Huang and C. Chen, "Denoising of partial discharge based on empirical mode decomposition", *Automation of Electric Power Systems*, vol. 60, pp. 53-56, 2005.

[7] H. Li, Y. Sun and C. Xu, "Noise elimination of PD signals by independent component analysis", *Journal of Sichuan University (Engneering Science Editiion*, vol. 39, no. 6, pp. 143-148, 2007.

[8] X. Xiong, S. Yang and X. Zhou, "IMF-based denoising method for vibration signal in rotating machinery", *Journal of Zhejiang University (Engneering Science*, vol. 45, no. 8, pp. 1376-1381, 2011.

[9] J. Zhang, H. Chen and P. Zhou, "New de-noising method for partial discharge signals based on wavelet threshold", *Advanced Technology of Electrical Engineering and Energy*, vol. 36, no. 8, pp. 80-88, 2017.

[10] K. Zhou, Y. Huang, M. Xie, and H. Min, "Mixed noises suppression of partial discharge signal employing short-time singular value decomposition", *Transaction of China Electrotechnical Society*, vol. 34, no. 11, pp. 2435-2443, 2019.

[11] J. Xie, Y. Liu, L. Liu, L. Tang, G. Wang, and X. Li, "A partial discharge signal denoising method based on adaptive weighted framing fast sparse representation", *of the CSEE*, vol. 39, no. 21, pp. 6428-6439, 2019.

[12] M. Ashtiani and S. Shahrtash, "Partial discharge de-noising employing adaptive singular value decomposition", *IEEE Transactions on Dielectrics Electrical Insulation*, vol. 21, no. 2, pp. 775-782, 2014.

[13] M. Xie, K. Zhou, Y. Huang, M. He, and X. Wang, "A white noise suppression method for partial discharge based on short time singular value decomposition", *Proceedings of the CSEE*, vol. 39, no. 3, pp. 915-922, 2019.

[14] H. Wei, H. Ma, T. Huang, and H. Huang, "Application of ICA de-noise method based on EMD in partial discharge signal of switch cabinet in power plant", *Proceedings of the CSU-EPSA*, vol. 31, no. 5, pp. 110-116, 2019.

[15] J. Zhong, X. Bi, Q. Shu, D. Zhang, and X. Li, "An improved wavelet spectrum segmentation algorithm based on spectral kurtogram for denoising partial discharge signals", *IEEE Transactions on Instrumentation and Measurement*, vol. 70, Article ID 3514408, 2021.

[16] C. Wu, Y. Gao, R. Wang, K. Wang, S. Liu, Y. Nie, and P. Wang, "Partial Discharge Detection Method Based on DD-DT CWT and Singular Value Decomposition", *Journal of Electrical Engineering Technology*, vol. 17, pp. 2433-2439, 2022.

[17] F. Miao and R. Zhao, "A new method of vibration signal denoising based on improved wavelet", *Journal of Low Frequency Noise*, Vibration and Active Control, vol. 41, no. 2, pp. 637-645, 2022.

[18] X. Song, C. Zhou, D. Hepburn, G. Zhang, and M. Michel, "Second generation wavelet transform for data denoising in PD measurement", *IEEE Transactions on Dielectrics and Electrical Insulation*, vol. 14, no. 6, pp. 1531-1537, 2007.

[19] A. Kyprianou, P. L. L. V. Efthimiou, A. Stavrou, and G. E. Georghiou, "Wavelet packet denoising for online partial discharge detection in cables and its application to experimental field results", *Measurement Science and Technology*, vol. 17, no. 9, pp. 2367-2379, 2006.

[20] J. Long, X. Wang, D. Dai, M. Tian, G. Zhu, and J. Zhang, "Denoising of UHF PD signals based on optimised VMD and wavelet transform", *IET Science Measurement Technology*, vol. 11, no. 6, pp. 753-760, 2017.

[21] D. L. Donoho, "De-noising by soft-thresholding", *IEEE Transactions on Information Theory*, vol. 41, no. 3, pp. 613-627, 1995.

[22] P. Chen and I. W. Selesnick, "Group-sparse signal denoising: non-convex regularization, convex optimization", *IEEE Transactions on Signal Processing*, vol. 62, no. 13, pp. 3464-3478, 2014.

[23] M. Protter, I. Yavneh, and M. Elad, "Closed-form MMSE estimation for signal denoising under sparse representation modeling over a unitary dictionary", *IEEE Transactions on Signal Processing*, vol. 58, no. 7, pp. 3471-3484, 2010.

[24] D. Moloney, D. Geraghty, C. Mcsweeney, and C. Mcelroy, "Streaming sparse matrix compression/decompression", *Lecture Notes in Computer Science*, vol. 3793, pp. 116-129, 2005.

[25] J. Wright, A. Y. Yang, A. Ganesh, S. S. Sastry, and Y. Ma, "Robust face recognition via sparse representation", *IEEE Transactions on Pattern Analysis and Machine Intelligence*, vol. 31, no. 2, pp. 210-227, 2009.

[26] I. W. Selesnick, "Sparse Regularization via convex analysis", *IEEE Transactions on Signal Processing*, vol. 65, no. 17, pp. 4481 -4494, 2017.

[27] S. Wang, I. W. Selesnick, G. Cai, B. Ding, and X. Chen, "Synthesis versus analysis priors via generalized minimax- concave penalty for sparsity-assisted machinery fault diagnosis", *Mechanical systems and signal processing*, vol. 127, pp. 202-233, 2019.

[28] O. P. Goswami, A. Shukla, and M. Kumar, "Optimal design and low noise realization of digital differentiator", *Journal of Electrical Engineering*, vol. 73, no. 5, pp. 332-336.

[29] Z. Jin, A. Dong, M. Shu, and Y. Wang, "Sparse ECG denoising with generalized minimax concave penalty", *Sensors*, vol. 19, no. 7, Article ID 1718, 2019.

Received 17 October 2022

Xuejun Chen was born in Quanzhou, China, in 1980. He received the MSc degree in test measurement technology and Instruments from Chongqing University of Technology, Chongqing, China, in 2007, and the PhD degree in Electrical engineering from State Key Laboratory of Power Transmission Equipment &System Security and New Technology, Chongqing University, Chongqing, China, in 2011. He is currently a Full Professor with the Key Laboratory of Fujian Universities for New Energy Equipment Testing, Putian University, Putian, China. His research interests include signal processing, fault diagnosis, vibration, health status assessment.

Li Ma received the BE degree from Henan University of Science and Technology, Luoyang, China in 2020. He is currently pursuing the MS degree in School of Mechanical Engineering and Automation, Fuzhou University, Fuzhou, China. His research interests are finite element analysis of electrical equipment.

Lei Zhang received the BE degree from Nanjing Agricultural University, Nanjing, China in 2021. He is currently pursuing the MS degree in college of Mechanical and Electrical Engineering, Fujian Agriculture and Forestry University, Fuzhou, China. His research interests are applications, testing, and fault diagnosis of electrical equipment.

Jianhuang Zhuang received the BE degree from School of Electrical Engineering, Fuzhou University, Fuzhou, China in 2005. He is currently a senior engineer with Putian power supply company of State Grid Fujian Electric Power Co., Ltd, Putian, China. His research interests are signal processing, fault diagnosis, and health status assessment.